Journal of Alloys and Compounds 692 (2017) 294–300

Contents lists available at ScienceDirect

Journal of Alloys and Compounds

journal homepage: http://www.elsevier.com/locate/jalcom

Platinum-decorated Cu(InGa)Se_2/CdS photocathodes: Optimization of Pt electrodeposition time and pH level

Min-woo Kim [a, 1], Hyun Yoon [b, 1], Tae Yoon Ohm [a], Mukund G. Mali [a], Sung Kyu Choi [c], Hyunwoong Park [c], Salem S. Al-Deyab [d], Dong Chan Lim [e, *], SeJin Ahn [f, *], Sam S. Yoon [a, *]

[a] School of Mechanical Engineering, Korea University, Seoul, 136-713, Republic of Korea
[b] KIER-UNIST Advanced Center for Energy, Korea Institute of Energy Research (KIER), 50, UNIST-gil, Ulsan, 44919, Republic of Korea
[c] School of Architectural, Civil, Environmental, and Energy Engineering, Kyungpook National University, Daegu, 41566, Republic of Korea
[d] Petrochemical Research Chair Chemistry Department, College of Science, King Saud University, P.O. Box 2455, Riyadh, 11451, Saudi Arabia
[e] Surface Technology Division, Korea Institute of Materials Science, Changwon, 641-010, Republic of Korea
[f] Photovoltaic Laboratory, Korea Inst. of Energy Research, 71-2 Jangdong, YuseongGu, DaeJeon 305-543, Republic of Korea

ARTICLE INFO

Article history:
Received 8 July 2016
Received in revised form
26 August 2016
Accepted 30 August 2016
Available online 31 August 2016

Keywords:
CIGS/CdS
Photocurrent
Platinum
p-n junction
Water splitting

ABSTRACT

Photoelectrochemical (PEC) water splitting was performed using co-evaporated Cu(In,Ga)Se_2 (CIGS, p-type) films as the photocathode. Pt was electrodeposited on CIGS and CIGS/CdS films. The effect of the electrodeposition time was investigated to determine the optimal deposition conditions. The CIGS film was covered with a 60-nm-thick CdS layer (n-type) using a chemical-bath deposition technique, which created a p-n junction. The effect of the Pt electroplating time was again investigated for the CIGS/CdS films; thus, the effect of CdS addition could be quantitatively investigated. The effect of the pH of 0.5 M Na_2SO_4 electrolyte was also investigated. The optimal water-splitting performance occurred at −24.16 mA/cm^2 at −0.7 V vs. Ag/AgCl with a Pt electrodeposition time of 20 min and pH 9. The CIGS/CdS films were characterized by X-ray diffraction, scanning electron microscopy, and focused-ion beam transmission electron microscopy.

1. Introduction

Solar energy can potentially replace traditional fossil fuels and fulfill the ever growing need for energy on a global scale. While photoelectrochemical (PEC) cells for solar reduction of CO_2 are still in their infancy with solar-to-fuel (STF) efficiencies below 0.2% [1], the PEC water-splitting technology can generate hydrogen energy using solar light in a sustainable manner and is thus considered a prospective route for meeting the global energy needs [2,3]. Gaseous hydrogen is produced by placing a semiconducting material in water under light illumination. Since the first report on the photoelectrolysis of titania (TiO_2) by Fujishima and Honda [4], various attempts have been made to achieve efficient solar water splitting to produce hydrogen. However, the poor solar-to-hydrogen (STH) efficiency of titania and other equivalent semiconducting materials has hindered their use at a commercial level. Therefore, new materials capable of achieving greater solar-to-hydrogen efficiencies are needed.

An ideal photoelectrode material must be electrochemically stable, possess a high STH efficiency, and have a suitable band gap. Ideally, photo-electrode materials should be operative in the visible light range. For successful water splitting, the maximum energy of the valence band of a photoelectrode must be below the oxidation potential of the water molecule reaction (O_2/H_2O), and that of the conduction band must be above the reduction potential of the H^+ ion reaction (H^+/H_2). The theoretical minimum free energy required to split water is 1.23 eV. Hence, the minimum bandgap of a photoelectrode material must be greater than 1.23 eV. However, considering the irreversibilities that arise from the electrochemical reactions and mesoscale heat-transfer effects, it would be desirable for the material to have a band gap in the range of 1.6–1.9 eV $CuInGaSe_2$ (or CIGS) solar cells, which have a tunable band gap in the range of 1–2.4 eV, meet this requirement [5].

Metal oxides such as $BiVO_4$, WO_3, TiO_2, and Fe_2O_3 are considered photoanode materials, while Cu_2O, GaAs, GaP, SiC, and CIS are

* Corresponding authors.
E-mail addresses: dclim@kims.re.kr (D.C. Lim), swisstel@kier.re.kr (S. Ahn), skyoon@korea.ac.kr (S.S. Yoon).
[1] These authors have contributed equally.

http://dx.doi.org/10.1016/j.jallcom.2016.08.313
0925-8388/

considered photocathode materials. Hara et al. fabricated a film with Cu_2O powder for water splitting [6]. Kargar et al. fabricated a solution-grown Cu_2O network in three dimensions for water splitting [7]. However, the relatively high band gap of copper oxide, which is in the range of 2.0–2.2 eV, limited the efficient absorption of visible light [8]. To circumvent this issue, Luo et al. transformed Cu_2O into $CuInS_2$ to improve the water-splitting performance [9]. The band gap of CIS-type materials is well-suited for the photocathode applications [10,11]. Yokoyama et al. [12] fabricated CIGS thin films using a molecular beam epitaxy technique. Pt was coated onto the CIGS film, and the photocurrent density (PCD) of the film was measured. However, CIGS is a p-type absorbent layer. One of the main purposes of using CIGS as a photocathode is to provide autonomously supplied voltage, which negates the need for external voltage. To achieve this, CIGS should be fabricated into a complete p-n junction, in which the n-type CdS should be deposited on top of the p-type CIGS layer. This type of p-n junction can be potentially used as a part of a stand-alone H_2 production device without the need of external voltage supply. Furthermore, it is important to understand the PEC performance as a function of the pH level and the Pt catalyst amount, which determines the interfacial phenomena such as band-bending and the amount of H^+ ions generated during the electrochemical reactions [13]. Pt not only promotes the hydrogen production, but also suppresses the recombination. Herein, we investigate the effect of the pH of the electrolyte and Pt electrodeposition time on the PEC properties of a CIGS/CdS cell working as a p-n junction. The CIGS layer was fabricated by co-evaporation, and the CdS layer was deposited using a chemical-bath deposition technique. The material was characterized by scanning electron microscopy (SEM), X-ray diffraction (XRD), and focused-ion beam (FIB) transmission electron microscopy (TEM). The actual production of hydrogen bubbles was confirmed and visualized using a CCD camera. The quantitative PCD values were measured while varying the pH of the electrolyte and Pt electroplating time. The optimal pH value and Pt coating time were determined.

2. Experimental

2.1. Fabrication of CIGS/CdS films

A Mo back contact with a thickness of 1.1–1.2 μm was deposited on a soda-lime glass substrate using DC magnetron sputtering. The CIGS layer was grown using a three-stage process involving the co-evaporation of In, Ga, Cu, and Se [14]. In the first stage, an $(In_{0.7},Ga_{0.3})_2Se_3$ layer with a thickness of 1 μm was grown by co-evaporating In, Ga, and Se onto the Mo/glass substrates at 400 °C. In the second stage, a CIGS film was formed by evaporating Cu and Se onto the $(In,Ga)_2Se_3$ layer at 550 °C. The end of the second stage was determined by measuring the substrate temperature drop. At the point when the substrate temperature decreased, CIGS had a slightly Cu-poor composition, i.e., $Cu/(In + Ga) < 1$. After this change, more Cu was added and the $Cu/(In + Ga)$ ratio was adjusted to 1.3 after the second stage. Because only Cu and Se were supplied during the second stage, the surface region contained a small amount of $Cu_{2-x}Se$. In the third stage, In, Ga, and Se elements were evaporated onto the CIGS layer to convert the Cu-rich film to a Cu-poor film. A CdS buffer layer (60 nm thick) was deposited onto the CIGS films by chemical-bath deposition using $CdSO_4$ (0.0015 M), NH_4OH (0.01 M), and a thiourea (0.05 M) aqueous solution.

2.2. Electrodeposition of the Pt co-catalyst

To enhance the kinetics of the water-reduction reaction, platinum nanoparticles were potentiostatically electrodeposited in the dark from a solution of 1 mM H_2PtCl_6 in deionized water at −0.1 V versus Ag/AgCl for 10, 20, and 30 min.

2.3. Material characterization

The crystallinity of the CIGS film was studied using X-ray diffraction (XRD, Rigaku, Tokyo, Japan, D/max-2500, Cu K radiation over a 2θ range of 20°–80°). The morphologies of the CIGS and CIGS/CdS–Pt films were studied using high-resolution scanning electron microscopy (FE-SEM; S-5000, Hitachi, Japan) at 10 kV and focused-ion beam transmission electron microscopy (FIB-TEM). The effective film thickness was determined by averaging five different measurements to confirm the statistical reliability.

2.4. Photoelectrochemical measurements

For all our PEC measurements, a single cell with three electrodes was used, as depicted in Fig. 1. The CIGS and CIGS/CdS–Pt films were used as the working electrode while an Ag/AgCl rod and platinum wire were used as the reference and counter electrodes, respectively. These three electrodes were placed 15 mm apart from each other, and their positions were fixed in order to acquire consistent data and minimize any transport limitations in the electrolyte. A 0.5 M Na_2SO_4 (pH = 1, 7, and 9) solution was used as the electrolyte. Nitrogen gas was purged through the electrolyte solution to remove any dissolved oxygen before the measurements. Artificial sunlight from a xenon arc lamp (Newport, Oriel Instruments, USA) equipped with an A.M. 1.5 filter was used as the light source with an intensity of 100 mW/cm^2. All the photocurrent data were recorded using a potentiostat (VersaSTAT-3, Princeton Applied Research, USA) with a scan rate of 10 mV/s with the applied voltage between 0.5 and −0.7 V.

3. Results and discussion

3.1. Characterization

According to our previous study [15], The crystalline structure of the current CIGS film, which has a band gap of about 1.18 eV, was characterized by XRD. The experiment was performed in the range of $10° < 2\theta < 80°$. The resulting spectrum is displayed in Fig. 2. Considering that the CIGS layer was co-evaporated onto a Mo substrate, a Mo peak was observed at $2\theta = 40°$. The peaks at $2\theta = 27.05°$, 44.88°, and 53.19° correspond to the (112), (220/204), and (312/116) planes, respectively, and confirm the crystallinity of the CIGS film. The polycrystalline structure of the CIGS film with a chalcopyrite crystal structure without the formation of any other phase was confirmed by Fig. 2.

The Raman spectra of the CIGS and CIGS/CdS thin films are shown in Fig. 3. The peak at 174 cm^{-1} confirmed the A1 mode of the chalcopyrite structure of the film. The broad peak at 215 cm^{-1} appeared because of the presence of the B2 mode [16]. The presence of CdS in the CIGS/CdS film was confirmed by the peak at 296 cm^{-1}, which corresponds to the typical LO (longitudinal optical) phonon of CdS.

The surface morphology of the films was studied using FE-SEM. Fig. 4 shows the cross-sectional and surface views of the CIGS, CIGS/CdS, and CIGS/CdS–Pt films from left to right, respectively. The cross-sectional views confirm the deposition of CIGS, CIGS/CdS, and CIGS/CdS–Pt layers on the Mo substrate, which were about 1.5 μm thick. The CIGS layer was about 2 μm thick and was densely coated with no signs of porosity. The grain size was fairly large (in the range of 200–500 nm) suggesting its potential to yield high STF efficiency. The n-type CdS layer, which was about 60 nm thick, was deposited via the chemical-bath deposition technique. The CdS

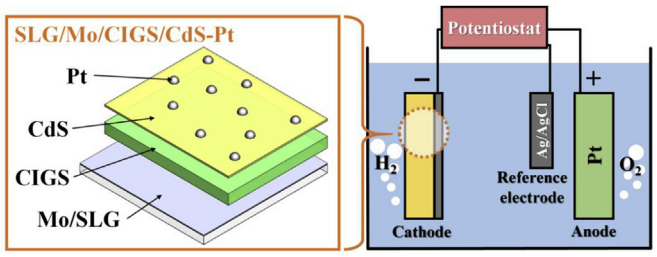

Fig. 1. Schematic of the water-splitting setup.

layer covered the homogeneously distributed angular grains of CIGS. Fig. 4c shows that Pt was deposited on the CIGS/CdS layer as a catalyst to enhance the hydrogen production. The CdS layer was textured and coated with Pt nanoparticles, which were sparsely deposited with an electrodeposition time of about 20 min. Excessive electrodeposition time caused the aggregation of the Pt particles and had an adverse effect on the overall PEC performance, which will be discussed in detail later.

Fig. 5 shows the cross-sectional FIB-TEM images of the CIGS/CdS film. The chemical bath-deposited CdS layer can be observed at the top of the film. The Cd layer followed the surface morphology of the CIGS layer, which had an uneven surface because of an imperfect coating during the co-evaporation process. The presence of Mo in the bottom layer is also evident.

3.2. Photoelectrochemical performance

The photocurrent generated by the CIGS photocathode was directly proportional to the rate of water reduction. The photocurrents measured with respect to the silver reference electrode were converted to the photocurrents vs. a reversible hydrogen electrode (RHE) using the following equation:

$$E_{RHE} = E_{Ag/AgCl} + 0.059pH + E_{Ag/AgCl^0}. \quad (1)$$

The current-potential curve for the pure CIGS film from Fig. 6 was measured in a 0.5 M Na_2SO_4 electrolyte at pH 9. The negative photocurrent value approached −0.2 mA/cm^2 at −0.7 V vs. Ag/AgCl, which is consistent with the typical photocurrent value for a p-type electrode. The onset photocurrent was observed at −0.4 V. This photocurrent value of the pure CIGS film (−0.2 mA/cm^2) is relatively low; this confirms the inability of the pure CIGS film to drive water reduction because of poor charge-carrier separation [17].

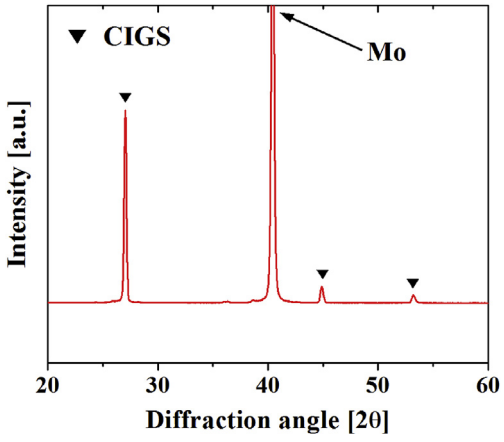

Fig. 2. XRD spectrum of the CIGS film.

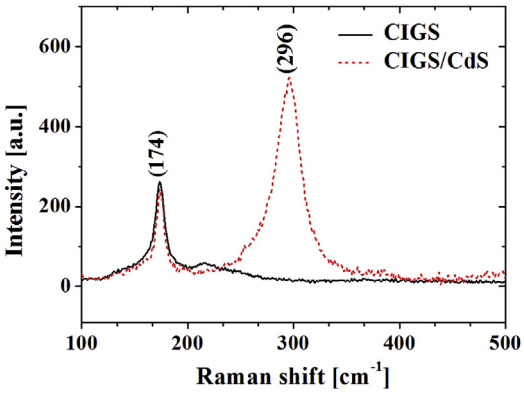

Fig. 3. Raman spectra of CIGS and CIGS/CdS films.

Given that the minimum theoretical free energy for water splitting is 1.23 eV, the CIGS band gap value of 1.2 eV also contributes to its poor water-splitting performance. In addition, the valence and conduction band potentials were not able to drive efficient water reduction and oxidation processes.

Pt is commonly used as a hydrogen evolution catalyst (HEC) and improves the reaction kinetics. Therefore, in order to improve the PCD, Pt was electrodeposited on the CIGS film. The CIGS film was immersed in a 1 mM H_2PtCl_6 solution mixed with deionized water to deposit Pt. The Pt deposition period was 20 min. Fig. 6 compares the photocurrents of the pure CIGS and CIGS/Pt films. The observed photocurrent for the CIGS/Pt film was −3.0 mA/cm^2, which indicates that the photocurrent was significantly improved by Pt deposition. When Pt was deposited on the CIGS film for 20 min, sparsely-grown Pt dots were observed on the CIGS film. The rough surface of the CIGS/Pt film was in direct contact with the electrolyte, which promoted the interfacial photocatalytic activities [18,19]. The Pt dots provided a continuous energetic state, which facilitated the efficient transport of large number of electrons during the redox reaction.

The addition of a CdS layer onto a CIGS layer should improve the PCD because it would generate a p-n junction. The band edge position of CdS is suitable for the hydrogen evolution reaction. When a CIGS/CdS p-n junction is used as a photocathode, CIGS acts as an efficient light absorber and generates electron–hole charge-carrier pairs while CdS subsequently separates the electrons and holes generated as a result of the light absorption [12,17]. The current-potential curve of the CIGS/CdS films is shown in Fig. 7. As expected, the PCD was significantly higher than that obtained for the films without the CdS layer (for the CIGS films shown in Fig. 6).

Fig. 7 shows the effect of the Pt electrodeposition time on the PCD. All the measurements were carried out at pH 9. The dark current values were near zero for all the cases. All the tested films exhibited the typical negative value of the cathodic PCD under light-illumination. All the PCD values under light-illumination were recorded at −0.7 V vs. Ag/AgCl (corresponds to 0 V vs. RHE) and were found to be −13.10, −24.16, and −19.46 mA/cm^2 after 10, 20, and 30 min of Pt electrodeposition, respectively. It is clear that 20 min of Pt electrodeposition yielded the highest photocurrent value of −24.16 mA/cm^2. The largest electrodeposition time of 30 min had an adverse effect on the photocurrent. At 30 min of electrodeposition, the aggregation or clustering effect by the excessive Pt dots over the CdS surface prevented the absorption of sufficient light by the CIGS layer, which hindered the generation of electron-hole pairs. It is noteworthy that the onset potential shifted from −0.4 to −0.2 V when the CdS layer was added.

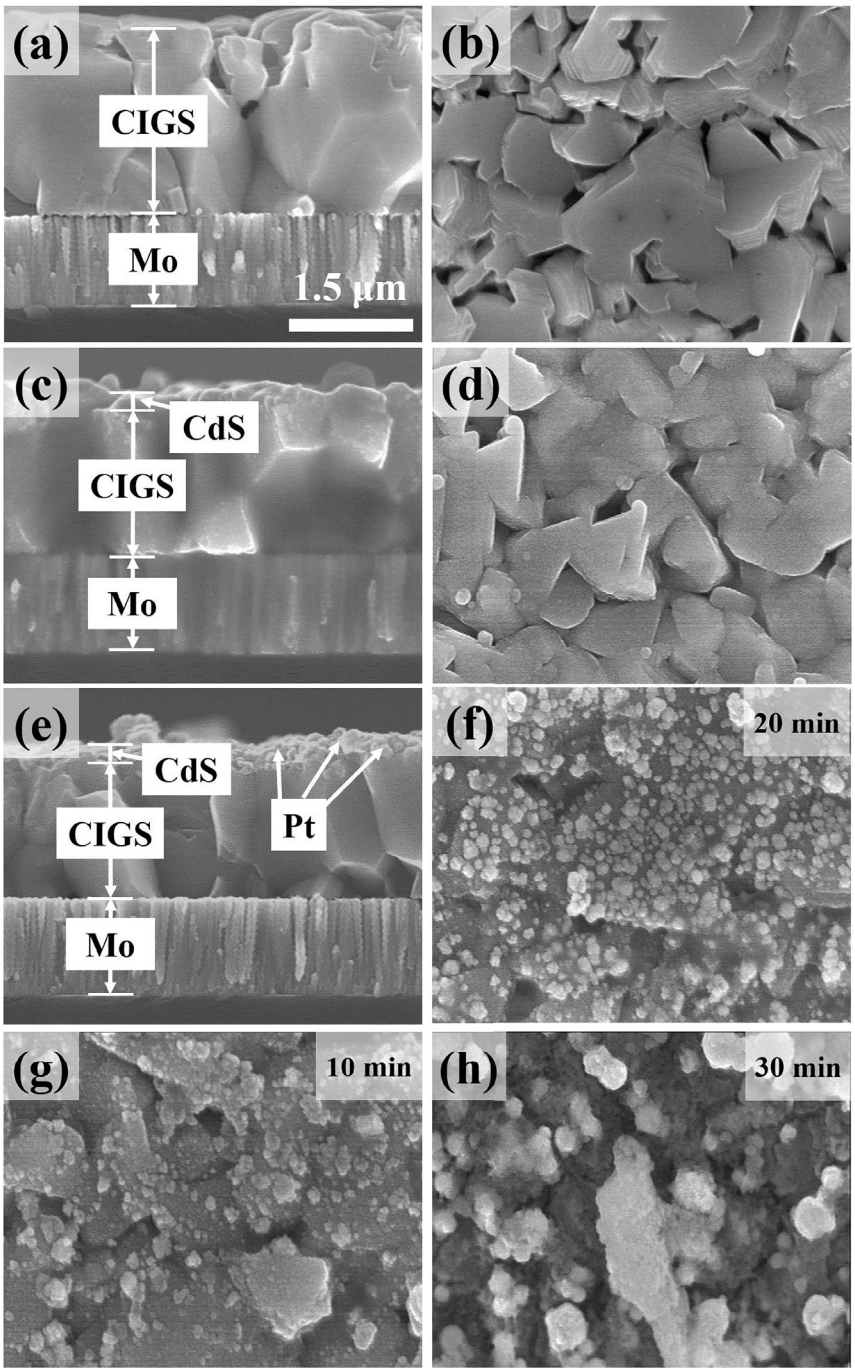

Fig. 4. (a) Cross-sectional and (b) surface images of a CIGS film. (c) Cross and (d) surface images of a CIGS/CdS film. (e) Cross and (f) surface images of a CIGS/CdS/Pt film with electroplating time (t_{ep}) of 20 min (g) and (h) Surface images of CIGS/CdS/Pt films with t_{ep} = 10 and 30 min, respectively.

The flat band potential (V_{fb}) of CIGS was measured by the Mott-Schottky analysis using the following equation:

$$\frac{1}{C^2} = \frac{2}{\varepsilon\varepsilon_0 e N_a}\left(\pm\left(V - V_{fb}\right) - \frac{kT}{e}\right)$$

where C is the capacitance, ε is the dielectric constant, ε_0 is the permittivity of vacuum (8.85×10^{-12} F/m), e is the electric charge (1.60×10^{-19} C), N_a is the acceptor concentration, V is the applied potential against Ag/AgCl electrode, k is the Boltzmann constant (1.38×10^{-23} J/K), T is the absolute temperature (298 K), and V_{fb} is the flat band potential. From this equation, the V_{fb} was determined by the linear extrapolation of the Mott-Schottky plot ($1/C^2$ vs. V) to intersect the voltage-axis at the value V_0. Fig. 8 shows the Mott-Schottky plot of CIGS. The experiments were performed in 0.5 M Na_2SO_4 solution at a frequency of 2512 Hz. The V_{fb} of the CIGS/CdS film was found to be −0.87 V vs. Ag/AgCl, while that of the CIGS/CdS/Pt film was found to be −0.44 V vs. Ag/AgCl.

The flat-band potentials of semiconductors indicate the position of their Fermi energy levels. The Fermi energy level of the CIGS/CdS film appeared to be at a considerably negative value. However, when Pt was electrodeposited on the CdS surface, the Fermi energy

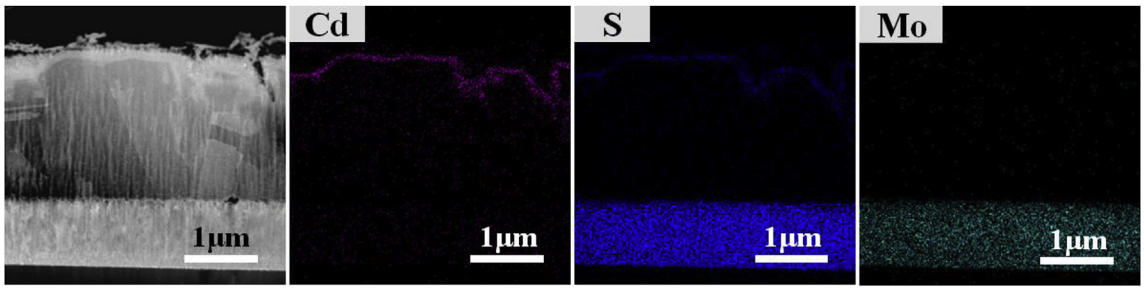

Fig. 5. Focused-ion beam (FIB) transmission electron microscopy (TEM) images of the CIGS/CdS solar cell sample.

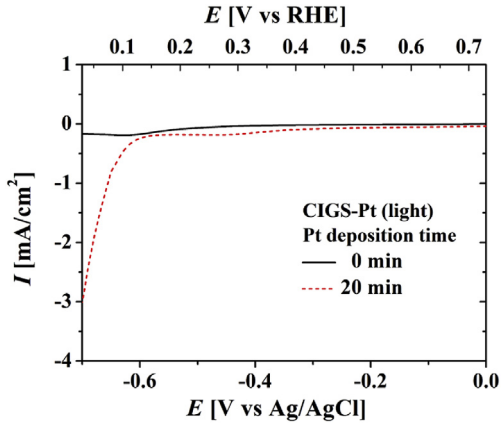

Fig. 6. Current-potential curve of pure CIGS and CIGS/Pt films measured in 0.5 M Na_2SO_4 at pH 9.

level shifted slightly towards the more positive potential, which in turn shifted the onset potential towards the right. This behavior is an indicative of the expedited electrochemical activity and can be explained by the band bending modification. The flat band potential shifting towards the more positive potential was observed at the semiconductor-metal interface, in which the flat band alignment arises when Pt was deposited on the CdS layer. The energy level of Pt (5.12–5.93 eV) is greater than the Fermi energy level of CdS (4.2–4.3 eV); hence the flat band of the CIGS/CdS/Pt photocathode shifts toward the more positive potential.

Fig. 9 shows the effect of the pH level of the Na_2SO_4 electrolyte used in the current experiment. The pH was adjusted to 1 by adding H_2SO_4, while the pH of 7, 9 and 11 was achieved by adding KOH. The electrodeposition time was fixed at its optimal time, which is 20 min according to Fig. 7. All the other experimental conditions were kept constant for consistent measurements. As shown in Fig. 9, the PCD values were −4.16, −16.81, −24.16 and −20.49 mA/cm^2 at pH values of 1, 7, 9 and 11, respectively; PCD in fact decreased

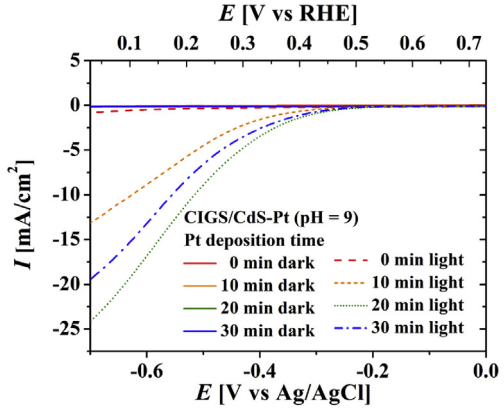

Fig. 7. Effect of Pt coating on the photocurrents of CIGS/CdS–Pt films.

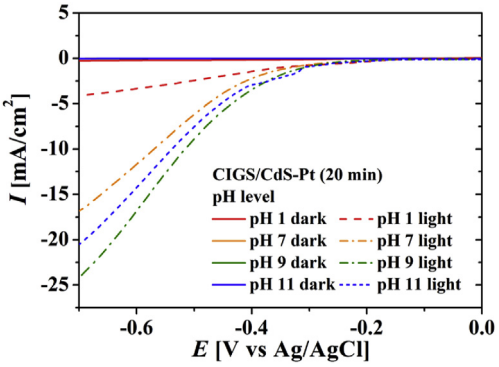

Fig. 9. Effect of pH of the electrolyte (0.5 M Na_2SO_4) on the photocurrents of the CIGS/CdS–Pt films. The electrodeposition time was fixed at 20 min.

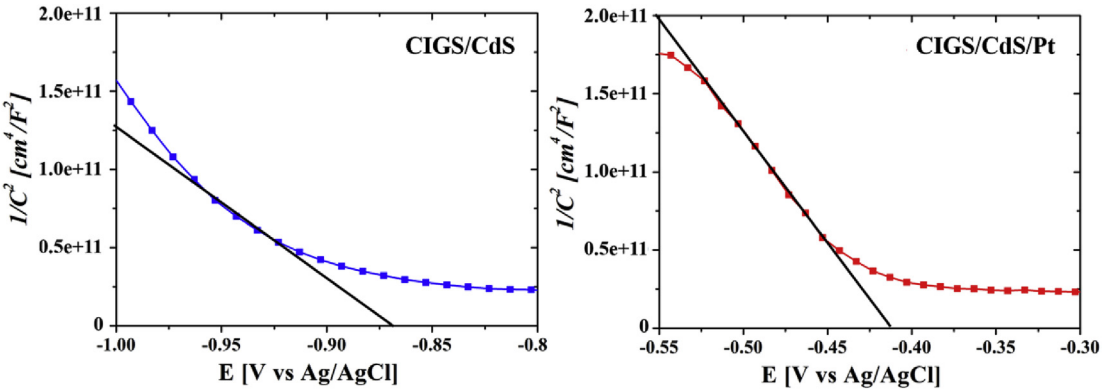

Fig. 8. Mott-Schottky plot of CIGS/CdS and CIGS/CdS/Pt films in 0.5 M Na_2SO_4 (pH 9) at a frequency of 2512 Hz.

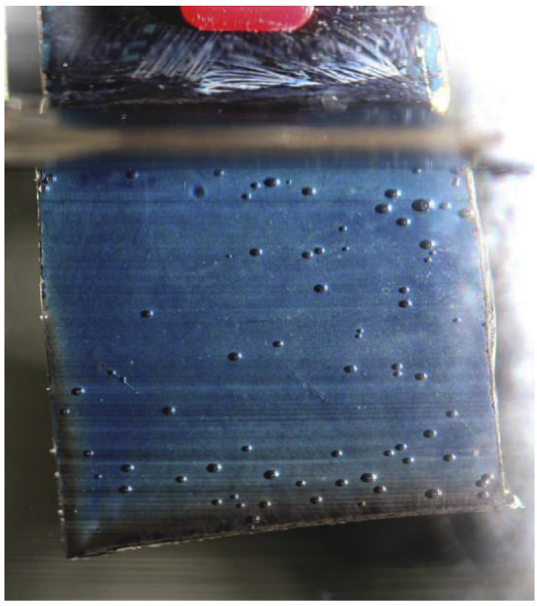

Fig. 10. Image showing H_2 evolution on the CIGS/CdS–Pt photoelectrode.

when the pH level increased from pH = 9 to 11. As such, the photocurrent value increased with the decreasing acidity of the electrolyte solution up to pH = 9. It is known that, under highly acidic conditions (pH = 1), the CIGS surface becomes more favorable for water reduction because of more number of H^+ ions, leading to a faster kinetic reaction [12]. However, in such a strong acidic environment, the photocathode is subjected to the oxidation and/or photo-corrosion of CdS. Furthermore, under acidic conditions such as the one used here, interactions between the SH^- groups of CdS and $PtCl_4^{2-}$ may lead to the formation of PtS, as illustrated below:

$$CdS + H_2O \rightarrow Cd(OH)^+ + SH^- \quad (2)$$

$$PtCl_6^{2-}(ad) + 2e^- \rightarrow PtCl_4^{2-}(ad) + 2Cl^- \quad (3)$$

$$PtCl_4^{2-}(ad) + SH^- \rightarrow PtS(s) + H^+ + 4Cl^- \quad (4)$$

The newly formed PtS reduces the CdS efficiency. Therefore, in a relatively acidic condition such as pH = 1, a lower photocurrent value may be obtained [20,21]. At pH = 7, the electrolyte yielded the lowest concentration of H^+/OH^- ions, which in turn formed a concentration gradient near the photocathode, where H^+ ions were removed for H_2 generation. This type of concentration gradient adversely affected the water reduction rate [12]. At the pH 9, a pronounced photocurrent increase was evident beyond the applied potential value of −0.4 V. The maximum PCD value was obtained at −0.7 V vs. Ag/AgCl, which corresponds to 0 V vs. RHE. The onset potentials for the CIGS/CdS–Pt films shifted towards the right as the pH increased from 1 to 11. This decreased the number of H^+ ions in the electrolyte solution. Such a shift in the onset potential towards the right is an indicative of the stiffer band-bending of CIGS.

Fig. 10 shows an image of the real-time H_2 production at the surface of the CIGS/CdS–Pt (20 min, pH = 9, and −0.7 V) photocathode. The size of the sample was 1 cm^2. At relatively high potentials in the range of −0.2–0.5 V, no hydrogen bubbles were seen. However, the hydrogen production started at −0.2 V and increased substantially at −0.7 V. The amount of the hydrogen bubbles increased considerably with an increase in the negative potential, which is consistent with the quantitative data shown in Fig. 7.

Fig. 11a and b describe the mechanism of charge transfer and separation at the CIGS-Pt and CIGS/CdS–Pt interfaces [17,22]. The addition of a layer of CdS to the CIGS layer forms a p-n junction. When this p-n junction photoelectrode (with further deposition of Pt co-catalyst) is immersed in a Na_2SO_4 electrolyte solution, the junction generates a depletion layer [2]. As observed from the CIGS/

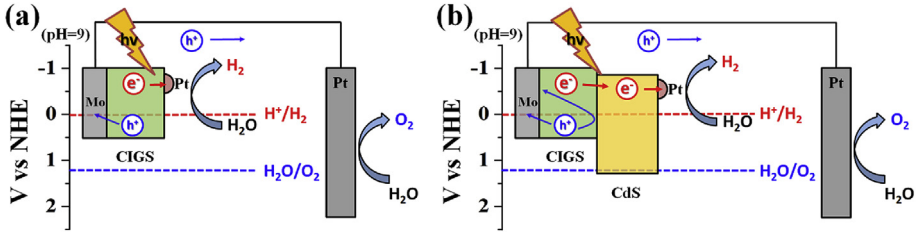

Fig. 11. Mechanism of charge transfer at (a) CIGS-Pt and (b) CIGS/CdS–Pt p-n junctions.

Table 1
Comparison of the PEC performance of the present CIGS/CdS–Pt photocathode with the literature data.

Photocathode	Electrolyte	pH of electrolyte	Applied potential	Photocurrent density [mA/cm^2]	Reference
CIGS/CdS–Pt (20 min)	**0.5**[a]	**9**	**−0.7**[d]	**−24**	**Present work**
CIGS/CdS/Mo/Pt	0.5[a]	6.8	0[e]	−30	Kumagai et al. [23]
CIGS/TiO_2/Pt	0.5[b]	0.3	−0.3[e]	−38	Azapira et al. [24]
CIGS/CdS/ZnO/TiO_2/Pt	0.5[b]	0	0[e]	−34	Luo et al. [25]
CGS/CdS–Pt	0.1[a]	9.5	0[e]	−9	Kumagai et al. [26]
CIS/CdS/TiO_2–Pt	0.1[c]	10	0[e]	−13	Zhao et al. [27]
CGS/CdS–Pt	0.1[a]	9	0[e]	−21	Moriya et al. [2]
CIGS/CdS–Pt	0.1[a]	9.5	0[e]	−12	Yokoyama et al. [12]

Bold indicates result of our present work.
[a] [Na_2SO_4].
[b] [H_2SO_4].
[c] [Na_2HPO_4].
[d] [V vs Ag/AgCl].
[e] [V vs RHE].

CdS–Pt band alignment shown in Fig. 11b, the depletion layer at the electrode-electrolyte interface for CIGS/CdS–Pt was thicker than that for bare CIGS-Pt (without CdS). This thicker depletion layer promoted the separation of the charge carriers (electrons) at the interface, resulting in greater hydrogen production. In addition, the difference between the valence band potentials of the CIGS and CdS layers also contributed to the enhancement of the electron transfer.

Table 1 compares the PCD value obtained in this work with those obtained previously. Our PCD value was fairly high among the available data. This high PCD value was achieved by optimizing the pH and the Pt electrodeposition time, indicating that the process optimization creates a room for the improvement in the PCD value. The presence of additional layers such as Mo, ZnO, and TiO_2 may promote the electron transfer from CIGS to the electrode-electrolyte interface while promoting the hole transfer from the CIGS absorber layer to the Mo substrate and eventually to the counter electrode. Therefore, these additional layers can increase the PCD value, which has been demonstrated by other authors [23–25]. Our current parametric studies suggest that the PCD values of CIGS films can be improved significantly by optimizing the pH of the electrolyte and/or Pt electroplating time.

4. Conclusion

Co-evaporated CIGS thin films were covered with a thin CdS layer via a chemical-bath deposition technique, thereby forming a p-n junction device for use in water splitting. The CIGS/CdS layers were electrodeposited with Pt for various deposition times. The resultant CIGS/CdS films were characterized by XRD, SEM, and FIB-TEM. We found that the Pt electrodeposition time of 20 min was optimal to yield the best PCD value of $-24.16\ mA/cm^2$. The effect of the pH on the PEC performance was also investigated, and pH 9 was found to be optimal. Thus, this study highlighted the combined effect of the pH of the electrolyte Pt deposition time on water splitting.

Acknowledgement

This research was supported by Global Frontier Program through the Global Frontier Hybrid Interface Materials (GFHIM) of the National Research Foundation of Korea funded by the Ministry of Science, ICT and Future Planning (2013M3A6B1078879) and the Industrial Strategic Technology Development Program (10045221) funded by the Ministry of Knowledge Economy. This work was also supported by the Technological Innovation R&D Program (S2314490) funded by the Small and Medium Business Administration. S.S. Yoon extends his appreciation to the Vice Deanship of Scientific Research chairs at King Saud University.

References

[1] J. Rongé, T. Bosserez, D. Martel, C. Nervi, L. Boarino, F. Taulelle, G. Decher, S. Bordiga, J.A. Martens, Monolithic cells for solar fuels, Chem. Soc. Rev. 43 (2014) 7963–7981.
[2] M. Moriya, T. Minegishi, H. Kumagai, M. Katayama, J. Kubota, K. Domen, Stable hydrogen evolution from CdS-modified $CuGaSe_2$ photoelectrode under visible-light irradiation, J. Am. Chem. Soc. 135 (2013) 3733–3735.
[3] J. Kim, T. Minegishi, J. Kobota, K. Domen, Enhanced photoelectrochemical properties of CuGa 3 Se 5 thin films for water splitting by the hydrogen mediated co-evaporation method, Energy Environ. Sci. 5 (2012) 6368–6374.
[4] A. Fujishima, K. Honda, Electrochemical photolysis of water at a semiconductor electrode, Nature 238 (1972) 37–38.
[5] H. Yoon, S.H. Na, J.Y. Choi, M.W. Kim, H. Kim, H.S. An, B.K. Min, S. Ahn, J.H. Yun, J. Gwak, K. Yoon, S.S. Kolekar, M.F.A.M. van Hest, S.S. Al-Deyab, M.T. Swihart, S.S. Yoon, Carbon- and oxygen-free Cu(InGa)(SSe)2 solar cell with a 4.63% conversion efficiency by electrostatic spray deposition, ACS Appl. Mater. Interfaces 6 (2014) 8369–8377.
[6] M. Hara, T. Kondo, M. Komoda, S. Ikeda, J.N. Kondo, K. Domen, M. Hara, K. Shinohara, A. Tanaka, Cu_2O as a photocatalyst for overall water splitting under visible light irradiation, Chem. Commun. (1998) 357–358.
[7] A. Kargar, S.S. Partokia, M.T. Niu, P. Allameh, M. Yang, S. May, J.S. Cheung, K. Sun, K. Xu, D. Wang, Solution-grown 3D Cu_2O networks for efficient solar water splitting, Nanotechnology 25 (2014) 205401.
[8] L. Rovelli, S.D. Tilley, K. Sivula, Optimization and stabilization of electrodeposited Cu_2ZnSnS_4 photocathodes for solar water reduction, ACS Appl. Mater. Interfaces 5 (2013) 8018–8024.
[9] J. Luo, S.D. Tilley, L. Steier, M. Schreier, M.T. Mayer, H.J. Fan, M. Grätzel, Solution transformation of Cu_2O into $CuInS_2$ for solar water splitting, Nano Lett. 15 (2015) 1395–1402.
[10] P. Jackson, D. Hariskos, R. Wuerz, O. Kiowski, A. Bauer, T.M. Friedlmeier, M. Powalla, Properties of Cu(In,Ga)Se_2 solar cells with new record efficiencies up to 21.7%, Phys. Status Solidi (RRL) – Rapid Res. Lett. 9 (2015) 28–31.
[11] P. Jackson, D. Hariskos, R. Wuerz, W. Wischmann, M. Powalla, Compositional investigation of potassium doped Cu (In, Ga) Se_2 solar cells with efficiencies up to 20.8%, Phys. Status Solidi (RRL)-Rapid Res. Lett. 8 (2014) 219–222.
[12] D. Yokoyama, T. Minegishi, K. Maeda, M. Katayama, J. Kubota, A. Yamada, M. Konagai, K. Domen, Photoelectrochemical water splitting using a Cu(In, Ga) Se_2 thin film, Electrochem. Commun. 12 (2010) 851–853.
[13] D.Y. Leung, X. Fu, C. Wang, M. Ni, M.K. Leung, X. Wang, X. Fu, Hydrogen production over titania-based photocatalysts, ChemSusChem 3 (2010) 681–694.
[14] S. Jung, S. Ahn, J.H. Yun, J. Gwak, D. Kim, K. Yoon, Effects of Ga contents on properties of CIGS thin films and solar cells fabricated by Co-evaporation technique, Curr. Appl. Phys. 10 (2010) 990–996.
[15] Y.-H. Seo, Y. Jo, Y. Choi, K. Yoon, B.-H. Ryu, S. Ahn, S. Jeong, Thermally-derived liquid phase involving multiphase Cu (In, Ga) Se_2 nanoparticles for solution-processed inorganic photovoltaic devices, RSC Adv. 4 (2014) 18453–18459.
[16] M. Li, M. Zheng, T. Zhou, C. Li, L. Ma, W. Shen, Fabrication and center-acterization of ordered $CuIn_{(1-x)}GaxSe_2$ nanopore films via template-based electrodeposition, Nanoscale Res. Lett. 7 (2012) 1–6.
[17] T.J. Jacobsson, C. Platzer-Björkman, M. Edoff, T. Edvinsson, $CuIn_xGa_{1-x}Se_2$ as an efficient photocathode for solar hydrogen generation, Int. J. Hydrogen Energy 38 (2013) 15027–15035.
[18] M. Szklarczyk, J.O.M. Bockris, Photoelectrocatalysis and electrocatalysis on p-Silicon, J. Phys. Chem. 88 (1984) 1808–1815.
[19] R.C. Rossi, N.S. Lewis, Investigation of the size-scaling behavior of spatially nonuniform barrier height contacts to semiconductor surfaces using ordered nanometer-scale nickel arrays on silicon electrodes, J. Phys. Chem. B 105 (2001) 12303–12318.
[20] H. Park, W. Choi, M.R. Hoffmann, Effects of the preparation method of the ternary CdS/TiO 2/Pt hybrid photocatalysts on visible light-induced hydrogen production, J. Mater. Chem. 18 (2008) 2379–2385.
[21] Q. Li, Z. Chen, X. Zheng, Z. Jin, Study of photoreduction of hexachloroplatinate (2-) on cadmium sulfide, J. Phys. Chem. 96 (1992) 5959–5962.
[22] M. Gloeckler, J.R. Sites, Efficiency limitations for wide-band-gap chalcopyrite solar cells, Thin Solid Films 480 (2005) 241–245.
[23] H. Kumagai, T. Minegishi, N. Sato, T. Yamada, J. Kubota, K. Domen, Efficient solar hydrogen production from neutral electrolytes using surface-modified Cu (In, Ga) Se 2 photocathodes, J. Mater. Chem. A 3 (2015) 8300–8307.
[24] A. Azarpira, M. Lublow, A. Steigert, P. Bogdanoff, D. Greiner, C.A. Kaufmann, M. Krüger, U. Gernert, R. van de Krol, A. Fischer, Efficient and stable TiO_2: Pt–Cu (in, Ga) Se_2 composite photoelectrodes for visible light driven hydrogen evolution, Adv. Energy. Mater. 5 (2015) 1402148.
[25] J. Luo, Z. Li, S. Nishiwaki, M. Schreier, M.T. Mayer, P. Cendula, Y.H. Lee, K. Fu, A. Cao, M.K. Nazeeruddin, Targeting ideal dual-absorber tandem water splitting using perovskite photovoltaics and CuInxGa1-xse2 photocathodes, Adv. Energy. Mater. 5 (2015) 1501520.
[26] H. Kumagai, T. Minegishi, Y. Moriya, J. Kubota, K. Domen, Photoelectrochemical hydrogen evolution from water using copper gallium selenide electrodes prepared by a particle transfer method, J. Phys. Chem. C 118 (2014) 16386–16392.
[27] J. Zhao, T. Minegishi, L. Zhang, M. Zhong, Gunawan, M. Nakabayashi, G. Ma, T. Hisatomi, M. Katayama, S. Ikeda, N. Shibata, T. Yamada, K. Domen, Enhancement of solar hydrogen evolution from water by surface modification with CdS and TiO_2 on porous $CuInS_2$ photocathodes prepared by an electrodeposition-sulfurization method, Angew. Chem. Int. Ed. 53 (2014) 11808–11812.